Polyhedral Rhenaborane Chemistry: Crystal and Molecular Structures of the *nido*-6-Rhenadecaborane Cluster Compounds [6,6,6,6-$(PMe_2Ph)_3$H-*nido*-6-ReB_9H_{13}] and [2-(PMe_2Ph)-6,6,6,6-$(PMe_2Ph)_2$ClH-*nido*-6-ReB_9H_{12}];† Nuclear Magnetic Resonance Parameters of These and Other Related *nido*-Rhenadecaborane Cluster Species

Michael A. Beckett, Norman N. Greenwood, John D. Kennedy, and Mark Thornton-Pett
Department of Inorganic and Structural Chemistry, University of Leeds, Leeds LS2 9JT

The compounds [6,6,6,6-$(PMe_2Ph)_3$H-*nido*-6-ReB_9H_{13}] (**1**) and [6,6,6,6-$(PMe_2Ph)_3$H-9-(OEt)-*nido*-6-ReB_9H_{12}] (**2**) are formed in 40 and 25% yields respectively from the reaction of *mer*-[$ReCl_3(PMe_2Ph)_3$] with an excess of [NEt_4][B_9H_{14}] in refluxing ethanol. Also obtained in smaller yields are an isomer of compound (**2**), [6,6,6,6-$(PMe_2Ph)_3$H-8-(OEt)-*nido*-6-ReB_9H_{12}] (**3**; *ca.* 4%), and a cluster-phosphine-substituted compound, [2-(PMe_2Ph)-6,6,6,6-$(PMe_2Ph)_2$ClH-*nido*-6-ReB_9H_{12}] (**4**; <1%). Compounds (**1**) and (**4**) have been structurally characterized by single-crystal *X*-ray diffraction methods. A chloro-substituted cluster compound, [2-Cl-6,6,6,6-$(PMe_2Ph)_3$H-*nido*-6-ReB_9H_{12}] (**5**) can be obtained essentially quantitatively from compound (**1**) by heating in *sym*-$C_2D_2Cl_4$ at *ca.* +100 °C; it is an isomer of compound (**4**). All the compounds are air-stable coloured crystalline solids and their formulation as *nido*-$B_{10}H_{14}$-like cluster compounds is consistent with their n.m.r. properties. The $(PMe_2Ph)_3$H groupings in compounds (**1**), (**2**), (**3**), and (**5**) exhibit a dual pseudo-rotational fluxionality with $\Delta G^{\ddagger}$ values of 45—60 and of *ca.* 30 kJ mol^{-1} respectively for the two sub-processes. The rhenium atoms in these cluster compounds can be considered to contribute three orbitals to the cluster bonding, and these plus the four ligands associated with the metal centres are in 'capped octahedral' type of configurations about the d^4 metal centres.

A number of 6-metalla-*nido*-decaborane species have been characterized [1-3] and in these the boron atom at the 6-position of the *nido*-$B_{10}H_{14}$ parent molecule has been notionally replaced by an isolobal metal centre which contributes three orbitals to the cluster bonding scheme. Examples have been reported for the transition elements manganese,[4,5] rhenium,[5] ruthenium,[6] cobalt,[7,8] rhodium,[9] and iridium.[9] In all of these clusters the metal centre has a straightforward octahedral six-orbital bonding configuration with a d^6 core. Here we report some new air-stable 6-rhenadecaborane *nido* ten-vertex clusters in which the metal atom is still a three-orbital cluster contributor, but in which the metal bonding environment now has a seven-orbital configuration with a d^4 core. This work includes the first reported structural studies on polyhedral rhenaborane species.

Results and Discussion

1. *General.*—The reaction of *mer*-[$ReCl_3(PMe_2Ph)_3$] with an excess of the *arachno*-[B_9H_{14}]$^-$ anion in refluxing ethanol results in two novel *nido*-6-rhenadecaborane cluster species, (**1**) and (**2**), as the major products [reaction (1)], plus other products

$$\textit{mer}\text{-}[ReCl_3(PMe_2Ph)_3] + [B_9H_{14}]^- \text{ (excess)} \longrightarrow \underset{(\mathbf{1})}{[(PMe_2Ph)_3HReB_9H_{13}]} + \underset{(\mathbf{2})}{[(PMe_2Ph)_3HReB_9H_{12}(9\text{-}OEt)]} \quad (1)$$

including (**3**) (4%, purple) and (**4**) (< 1%, blue). Both compounds (**1**) and (**2**) can be obtained in moderately good yields and can be formulated as [6,6,6,6-$(PMe_2Ph)_3$H-*nido*-6-ReB_9H_{13}] (**1**; a purple crystalline solid, 40%) and [6,6,6,6-$(PMe_2Ph)_3$H-9-(OEt)-*nido*-6-ReB_9H_{12}] (**2**; an orange crystalline solid, 25%). That these structures are correctly formulated follows from a single-crystal *X*-ray diffraction analysis of compound (**1**) (see section 2), elemental microanalysis (see Experimental section), and from comparative n.m.r. studies (see section 3). Two other *nido*-6-rhenadecaborane cluster compounds are formed in smaller yields in this reaction and one of these products (**3**; a purple crystalline solid, *ca.* 4%) is believed from n.m.r. studies to be a positional isomer of compound (**2**) with the ethoxy group now substituted in the 8-position of the *nido* ten-vertex cluster. Compound (**3**) can therefore be formulated as [6,6,6,6-$(PMe_2Ph)_3$H-8-(OEt)-*nido*-6-ReB_9H_{12}]. It is possible that compounds (**2**) and (**3**) are formed from the reaction of compound (**1**) with the solvent since (**1**) is the major product of the reaction and compounds (**2**) and (**3**) can be prepared from (**1**) by heating it in refluxing ethanol [reaction (2)]. However, the

$$\underset{(\mathbf{1})}{[(PMe_2Ph)_3HReB_9H_{13}]} \xrightarrow[1.5\text{ h, reflux}]{\text{EtOH}} \underset{(\mathbf{2})\ (ca.\ 5\%)}{[(PMe_2Ph)_3HReB_9H_{12}(9\text{-}OEt)]} + \underset{(\mathbf{3})\ (ca.\ 5\%)}{[(PMe_2Ph)_3HReB_9H_{12}(8\text{-}OEt)]} \quad (2)$$

higher yield of compound (**2**) when compared to compound (**3**) indicates that (**2**) may also be forming independently of (**1**) under the reaction conditions of equation (1).

The cluster electronic structure of these compounds appears to be very similar to that of previously reported d^6 iridium(III) species such as [6,6,6-$(PPh_3)_2$H-*nido*-6-IrB_9H_{13}][9] which also

† 6,6,6-Tris(dimethylphenylphosphine)-6-hydrido-*nido*-6-rhenadecaborane and 6-chloro-2,6,6-tris(dimethylphenylphosphine)-6-hydrido-*nido*-6-rhenadecaborane respectively.

Supplementary data available (No. SUP 56191, 6 pp.): anisotropic and isotropic thermal parameters. See Instructions for Authors, *J. Chem. Soc., Dalton Trans.*, 1985, Issue 1, pp. xvii—xix. Structure factors are available from the editorial office.

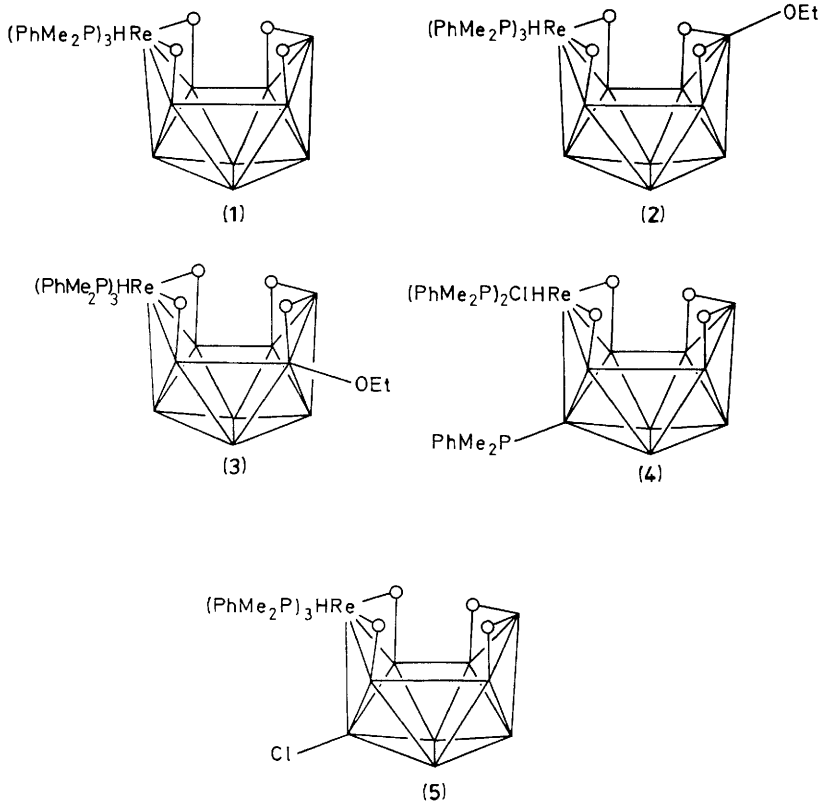

Figure 1. Schematic representations of the cluster structures of [6,6,6,6-$(PMe_2Ph)_3$H-*nido*-6-ReB_9H_{13}] (**1**), [6,6,6,6-$(PMe_2Ph)_3$H-9-(OEt)-*nido*-6-ReB_9H_{12}] (**2**), [6,6,6,6-$(PMe_2Ph)_3$H-8-(OEt)-*nido*-6-ReB_9H_{12}] (**3**), [2-(PMe_2Ph)-6,6,6,6-$(PMe_2Ph)_2$ClH-*nido*-6-ReB_9H_{12}] (**4**), and [2-Cl-6,6,6,6-$(PMe_2Ph)_3$H-*nido*-6-ReB_9H_{12}] (**5**). Each unsubstituted boron cluster vertex atom has an *exo*-terminal hydrogen atom bound to it (not shown)

have a metal–hydride hydrogen as well as two B–H–B and two M–H–B bridging hydrogen atoms. These iridium compounds readily lose dihydrogen quantitatively upon heating to give products, such as the *isocloso* compound $[(PMe_3)_2HIrB_9H_9]$, which are believed to have a seven-orbital d^4 iridium(v)-type metal bonding configuration.[10,11] It was therefore of interest to see whether compounds (**1**) and (**2**) would mirror this behaviour. Upon heating compound (**1**) in *sym*-$C_2D_2Cl_4$ a reaction did indeed occur and a purple crystalline solid [compound (**5**)] was formed in essentially quantitative yield [reaction (3)]. Interestingly, the reaction is one of chlorination by the solvent rather than cluster oxidation by loss of dihydrogen, and the structure of compound (**5**) can be deduced to be [2-Cl-6,6,6,6-$(PMe_2Ph)_3$H-*nido*-6-ReB_9H_{12}] by comparison of the n.m.r. data with those of [2-(PMe_2Ph)-6,6,6,6-$(PMe_2Ph)_2$ClH-*nido*-6-ReB_9H_{12}] (**4**). Compound (**4**) is another *nido*-6-rhenadecaborane that may be isolated in a small yield (< 1%) as a royal blue crystalline solid from reaction (1) and which has also been characterized by single-crystal *X*-ray diffraction analysis (section 2). Initial investigations indicate that, in the absence of chlorinating solvents, stronger heating of compound (**1**) and mild heating of compound (**2**) cause degradation processes resulting in the production of rhenaborane clusters with fewer than ten vertices and we hope to describe these products in future publications.

$$[(PMe_2Ph)_3HReB_9H_{13}] \xrightarrow[100\ °C]{C_2D_2Cl_4} [(PMe_2Ph)_3HReB_9H_{12}(2\text{-}Cl)] \quad (3)$$
(**5**) (*ca.* 100%, purple)

The cluster geometries of all five compounds are shown schematically in Figure 1. It is of interest to note that compounds (**4**) and (**5**) are positional isomers of one another, with (**4**) having a phosphine ligand bound to the boron cage and a chlorine atom bound to the metal centre whilst (**5**) has these interchanged.

The seven-orbital d^4 rhenium–hydride configuration (see following sections) reported here can be compared with the six-orbital d^6 structure of the previously reported[5] *nido*-6-rhenadecaborane anion $[6,6,6\text{-}(CO)_3\text{-}nido\text{-}6\text{-}ReB_9H_{13}]^-$. These compounds are related by an effective protonation ⟷ deprotonation process at the metal centre, the protonation activating one of the electron pairs of the d^6 core of the anion to partake in Re–H bonding. This appears to be primarily a metal-centred phenomenon which does not significantly affect the *nido* ten-vertex ReB_9 cluster bonding; for example the cluster ^{11}B n.m.r. properties, which would be expected to be very sensitive to cluster electronic changes, are very similar for the anionic species and the neutral hydride (see section 3). This constitutes a further example of the very flexible valence-shell electronic behaviour that is becoming increasingly recognized in many heavy transition-metal derivatives of binary boranes, and in particular, so far, those of iridium.[6,10–17]

2. *Discussion of Structures* (**1**)—(**5**) *and* X-*Ray Data of* (**1**) *and* (**4**).—The n.m.r. properties (see section 3) indicate that compounds (**1**)—(**5**) all have *nido*-6-metalladecaborane structures and this is confirmed by the results of single-crystal *X*-ray diffraction analyses on compounds (**1**) and (**4**). ORTEP drawings for [6,6,6,6-$(PMe_2Ph)_3$H-*nido*-6-ReB_9H_{13}] (**1**) and [2-(PMe_2Ph)-6,6,6,6-$(PMe_2Ph)_2$ClH-*nido*-6-ReB_9H_{12}] (**4**) are shown in Figures 2 and 3 respectively. Selected interatomic

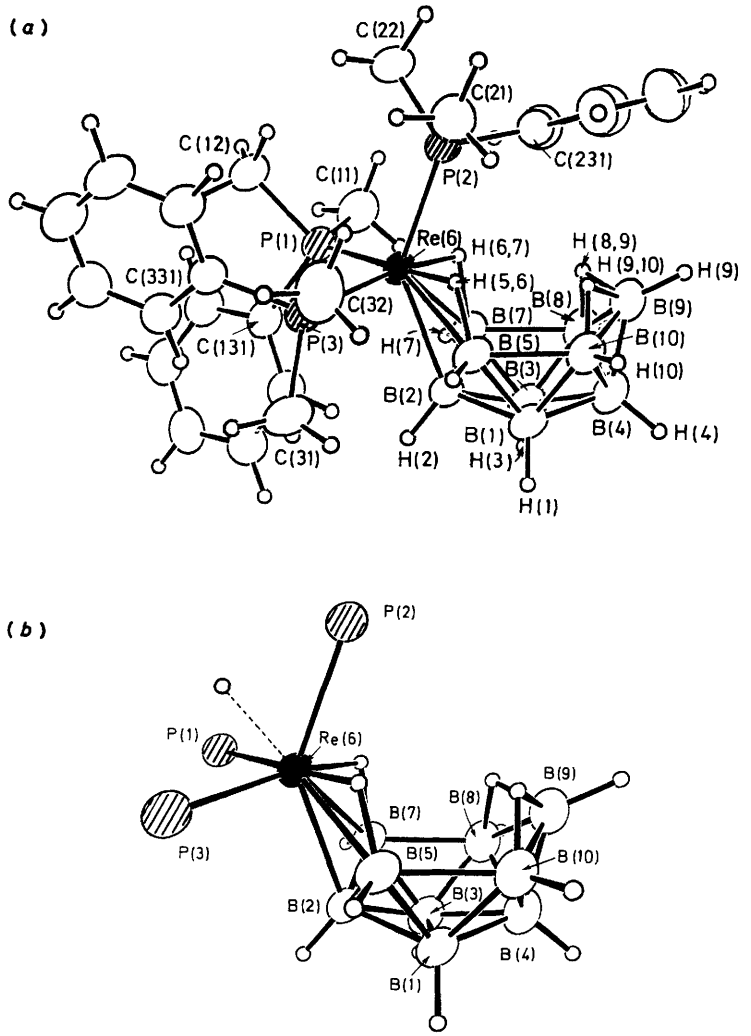

Figure 2. (*a*) Molecular structure of $[6,6,6,6\text{-}(PMe_2Ph)_3H\text{-}nido\text{-}6\text{-}ReB_9H_{13}]$ (**1**); all H atoms except Re(6)–H(terminal) were located. (*b*) Details of the metallaborane cluster with the hydrocarbon groups omitted. The Re(6)–H(terminal) atom (hatched line) is at the position inferred from geometrical and n.m.r. considerations

distances and interatomic angles for compound (**1**) are given in Tables 1 and 2, and the corresponding data for compound (**4**) are in Tables 3 and 4.

The geometry of the metallaborane clusters (**1**) and (**4**) is straightforward, being similar to that of previously reported *nido*-6-metalladecaboranes.[4–9] In particular the distances B(5)–B(10) and B(7)–B(8) of 209.4(8) and 201.0(7) pm [compound (**1**)] and 209.5(31) and 208.0(32) pm [compound (**4**)] are somewhat longer than those generally encountered in boron deltahedral clusters, diagnostic in this case of a *nido* ten-vertex formulation similar to that in *nido*-decaborane itself [B(5)–B(10) 197.3 pm].[18] Boron–boron distances in both of the clusters (**1**) and (**4**) are within the ranges quoted for other structurally characterized *nido*-6-metalladecaborane species.[4–9] The P(3)–B(2) distance of 194.9(19) pm in compound (**4**) is consistent with a bond order of one and is typical of a phosphorus atom directly bound to a cage boron atom.[6,11,19] No structural studies of polyhedral rhenaboranes have previously been reported, and so comparison with other rhenium–boron distances is not yet possible. The rhenium–boron distances in compound (**1**) [Re(6) to B(5) 236.6(5), to B(2) 237.8(5), and to B(7) 238.6(5) pm] and compound (**4**) [Re(6) to B(5) 232.7(21), to B(2) 232.0(19), and to B(7) 238.7(21) pm] are significantly longer than the corresponding iridium–boron distances in the iridadecaborane analogue $[6,6,6\text{-}(PPh_3)_2H\text{-}nido\text{-}6\text{-}IrB_9H_{13}]$ [Ir(6) to B(5) 228.9(9), to B(2) 226.9(8), and to B(7) 228.1(11) pm],[9] and also appear to be somewhat longer than the limited number of osmium–boron distances which have been reported and which are found to fall within the range 215(2)—228(2) pm.[11,20] The two metal-bound phosphorus atoms in compound (**4**) [P(1) and P(2)] are at an average distance of *ca.* 240 pm from Re(6) which is similar to that observed for two [P(1) and P(3)] of the three phosphorus atoms [P(1),P(2),P(3)] in compound (**1**) [P(1), 240.4(3); P(3), 240.0(3) pm]. The other phosphorus atom, P(2), is in the apical position and has a somewhat shorter bond length of 235.3(3) pm which may reflect the relative *trans* effects of Re–B(2) *versus* Re–H–B. In compound (**4**) the chlorine atom, Cl(1), is in the apical position at a distance of 250.1(7) pm from Re(6), which is rather long for a typical Re–Cl bond (235—245 pm).[21]

Of more interest is the geometry about the metal centres of compounds (**1**) and (**4**) and in particular the geometry of the non-borane ligands and their relationship to the disposition of the borane ligand. Unfortunately, the Re terminal hydrogen atom was not locatable in the diffraction analysis of either compound. However, in each case it is readily positioned from

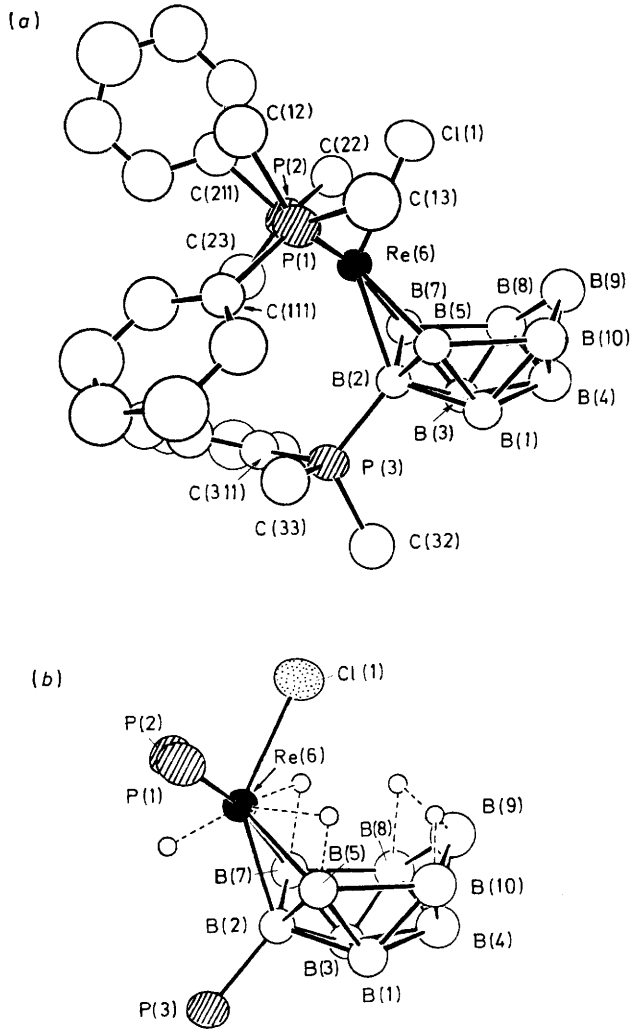

Figure 3. (*a*) Molecular structure of [2-(PMe_2Ph)-6,6,6,6-(PMe_2Ph)$_2$-ClH-*nido*-6-ReB_9H_{12}] (**4**); H atoms were not located. (*b*) Details of the metallaborane cluster with bridging and Re(6)–H(terminal) atoms (hatched lines) at positions inferred from geometrical and n.m.r. considerations, and from comparison with compound (**1**) (Figure 2). Each B atom except B(2) has an *exo*-terminal H atom bound to it (not illustrated)

a consideration of the n.m.r. properties (see Table 5 and discussion in section 3 which also considers the geometry of the remainder of the ligation sphere).

In the straightforward non-substituted species [Figures 1, (**1**), and 2] n.m.r. considerations indicate that the terminal hydride resides in a position which has *cisoid* characteristics with respect to all three phosphine ligands, and the large angles between the phosphorus–metal bond vectors (mean value *ca.* 103°) reasonably assign it to the position shown in (**B**) (Figure 4) in the solid-state structure determined by diffraction analysis. The geometry about the metal is then to be regarded as seven-orbital capped octahedral, with the three phosphine ligands occupying 'octahedral' positions, and the hydrogen atom occupying the fourth capping position; the remaining three octahedral positions are then taken by the two Re–H–B bridging bonds and by a 'bent' bond to B(2) which will have its maximum electron density in an *exo*-polyhedral region outside the Re(6)–B(2) vector.[9] In these terms the species can be considered as an 18-electron d^4 rhenium(III) complex in which the borane residue acts as an effective tridentate *arachno*-$[B_9H_{13}]^{2-}$ ligand

Table 1. Selected interatomic distances (pm) for [6,6,6,6-(PMe_2Ph)$_3$H-6-ReB_9H_{13}] (**1**) with estimated standard deviations (e.s.d.s) in parentheses

(*a*) From the rhenium atom			
Re(6)–P(1)	240.4(3)	Re(6)–B(2)	237.8(5)
Re(6)–P(2)	235.3(3)	Re(6)–B(5)	236.6(5)
Re(6)–P(3)	240.0(3)	Re(6)–B(7)	238.6(5)
Re(6)–H(5,6)	179.3(32)	Re(6)–H(6,7)	165.4(42)
(*b*) Boron–boron			
B(1)–B(2)	179.1(7)	B(2)–B(3)	177.4(7)
B(1)–B(3)	180.5(7)		
B(1)–B(5)	177.1(7)	B(3)–B(7)	176.5(7)
B(1)–B(4)	180.4(7)	B(3)–B(4)	179.1(8)
B(1)–B(10)	173.9(8)	B(3)–B(8)	175.1(8)
B(2)–B(5)	179.5(7)	B(2)–B(7)	180.5(7)
B(4)–B(9)	172.0(8)		
B(4)–B(8)	178.7(7)	B(4)–B(10)	178.1(8)
B(5)–B(10)	209.4(8)	B(7)–B(8)	201.0(7)
B(9)–B(10)	178.8(8)	B(8)–B(9)	179.7(8)
(*c*) Boron–hydrogen			
B(1)–H(1)	113.2(32)	B(3)–H(3)	107.1(34)
B(5)–H(5)	119.0(33)	B(7)–H(7)	109.3(34)
B(10)–H(10)	112.4(40)	B(8)–H(8)	103.1(43)
B(2)–H(2)	110.3(41)		
B(9)–H(9)	112.5(42)		
B(4)–H(4)	107.5(39)		
B(10)–H(9,10)	128.7(41)	B(8)–H(8,9)	124.5(37)
B(9)–H(9,10)	123.7(42)		
B(9)–H(8,9)	130.8(38)		

Table 2. Selected interatomic angles (°) for [6,6,6,6-(PMe_2Ph)$_3$H-6-ReB_9H_{13}] (**1**) with e.s.d.s in parentheses

(*a*) At the rhenium atom			
P(1)–Re(6)–P(2)	99.3	P(3)–Re(6)–P(2)	115.1
P(1)–Re(6)–P(3)	96.0		
P(1)–Re(6)–B(5)	84.8(2)	P(3)–Re(6)–B(7)	80.0(2)
P(1)–Re(6)–B(2)	107.8(2)	P(3)–Re(6)–B(2)	91.8(2)
P(1)–Re(6)–B(7)	151.1(1)	P(3)–Re(6)–B(5)	132.6(1)
P(2)–Re(6)–B(2)	139.5(1)		
P(2)–Re(6)–B(5)	111.5(2)	P(2)–Re(6)–B(7)	108.4(2)
P(1)–Re(6)–H(5,6)	83.6(11)	P(3)–Re(6)–H(6,7)	89.4(15)
P(1)–Re(6)–H(6,7)	174.6(14)	P(3)–Re(6)–H(5,6)	165.0(10)
P(2)–Re(6)–H(5,6)	79.6(11)	P(2)–Re(6)–H(6,7)	78.9(15)
B(5)–Re(6)–B(2)	44.4(1)	B(7)–Re(6)–B(2)	44.4(1)
B(5)–Re(6)–B(7)	77.5(2)		
(*b*) Rhenium–boron–boron			
Re(6)–B(5)–B(1)	122.0(3)	Re(6)–B(7)–B(3)	121.3(3)
Re(6)–B(5)–B(2)	68.4(2)	Re(6)–B(7)–B(2)	67.8(2)
Re(6)–B(5)–B(10)	121.2(2)	Re(6)–B(7)–B(8)	122.1(3)
Re(6)–B(2)–B(1)	119.9(3)	Re(6)–B(2)–B(3)	120.8(3)
Re(6)–B(2)–B(5)	67.2(2)	Re(6)–B(2)–B(7)	67.7(2)
(*c*) Other			
Re(6)–H(5,6)–B(5)	99.1(20)	Re(6)–H(5,6)–B(7)	109.5(28)
B(9)–H(9,10)–B(10)	90.2(28)	B(9)–H(8,9)–B(8)	89.4(24)
H(2)–B(2)–Re(6)	121.1(21)		

to the $[ReH(PMe_2Ph)_3]^{2+}$ centre. In cluster terms the neutral $ReH(PMe_2Ph)_3$ fragment may be regarded as isolobal and isoelectronic with the 6-BH vertex in *nido*-$B_{10}H_{14}$ in that it contributes three orbitals and two electrons to the *nido* ten-vertex cluster bonding.

Compound (**1**) is also interesting in that the crystal molecular structure does not represent the most stable species in solution.

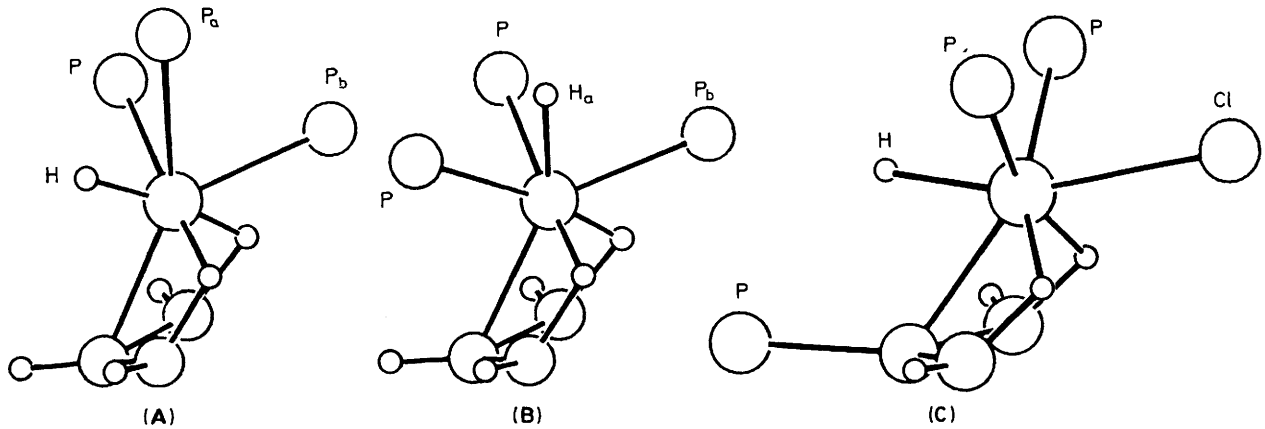

Figure 4. Representation of the proposed structures at the metal atom in $[(PMe_2Ph)_3HReB_9H_{13}]$ (**1**) [(**A**) and (**B**)] and $[(PMe_2Ph)_2ClHReB_9H_{12}(2\text{-}PMe_2Ph)]$ (**4**) [(**C**)]. Structure (**A**) is the most stable configuration in solution for compound (**1**), and (**B**) is as found in the solid state: both (**A**) and (**B**) have seven-orbital 'capped octahedral' metal bonding geometry (Figure 5) with P_a occupying the capping position in (**A**) and H_a in (**B**). In the low-temperature fluxional process P_b remains fixed and the other two phosphines and the terminal hydride interchange (Figure 8). At higher temperatures all three phosphines and the hydride interchange. For structure (**C**) see also Figure 5

Table 3. Selected bond lengths (pm) for $[2\text{-}(PMe_2Ph)\text{-}6,6,6,6\text{-}(PMe_2Ph)_2ClH\text{-}6\text{-}ReB_9H_{12}]$ (**4**) with e.s.d.s in parentheses

(*a*) From the rhenium atom			
Re(6)–P(1)	235.5(6)	Re(6)–P(2)	243.6(6)
Re(6)–Cl(1)	250.1(7)		
Re(6)–B(5)	232.7(21)	Re(6)–B(7)	238.7(21)
Re(6)–B(2)	232.0(19)		
(*b*) Boron–boron			
B(1)–B(2)	180.4(26)	B(2)–B(3)	182.2(26)
B(1)–B(3)	182.0(27)		
B(1)–B(5)	179.0(28)	B(3)–B(7)	177.2(27)
B(1)–B(4)	184.4(30)	B(3)–B(4)	181.2(29)
B(1)–B(10)	177.7(30)	B(3)–B(8)	175.8(29)
B(2)–B(5)	181.6(28)	B(2)–B(7)	178.9(26)
B(4)–B(9)	173.8(33)		
B(4)–B(8)	176.8(31)	B(4)–B(10)	182.4(32)
B(5)–B(10)	209.5(31)	B(7)–B(8)	208.0(32)
B(9)–B(10)	180.4(32)	B(8)–B(9)	181.9(33)
(*c*) Other			
P(3)–B(2)	194.9(19)		

Table 4. Selected interatomic angles (°) for $[2\text{-}(PMe_2Ph)\text{-}6,6,6,6\text{-}(PMe_2Ph)_2ClH\text{-}6\text{-}ReB_9H_{12}]$ (**4**) with e.s.d.s in parentheses

(*a*) At the rhenium atom			
P(1)–Re(6)–Cl(1)	83.9(3)	P(2)–Re(6)–Cl(1)	83.7(3)
P(1)–Re(6)–P(2)	106.3(3)		
P(1)–Re(6)–B(5)	88.4(6)	P(2)–Re(6)–B(7)	83.2(6)
P(1)–Re(6)–B(2)	120.7(5)	P(2)–Re(6)–B(2)	116.5(5)
P(1)–Re(6)–B(7)	165.2(5)	P(2)–Re(6)–B(5)	162.3(5)
Cl(1)–Re(6)–B(2)	137.4(4)		
Cl(1)–Re(6)–B(5)	108.0(6)	Cl(1)–Re(6)–B(7)	108.8(6)
B(5)–Re(6)–B(2)	46.0(6)	B(7)–Re(6)–B(2)	44.7(6)
B(5)–Re(6)–B(7)	80.5(7)		
(*b*) Rhenium–boron–boron			
Re(6)–B(5)–B(1)	119.3(13)	Re(6)–B(7)–B(3)	119.9(12)
Re(6)–B(5)–B(2)	66.3(9)	Re(6)–B(7)–B(2)	65.7(9)
Re(6)–B(5)–B(10)	117.1(11)	Re(6)–B(7)–B(8)	120.0(13)
Re(6)–B(2)–B(1)	119.0(11)	Re(6)–B(2)–B(3)	120.9(11)
Re(6)–B(2)–B(5)	67.2(9)	Re(6)–B(2)–B(7)	69.7(9)
(*c*) Other			
P(3)–B(2)–Re(6)	121.6(9)		
P(3)–B(2)–B(1)	108.8(12)	P(3)–B(2)–B(3)	110.7(12)
P(3)–B(2)–B(5)	118.7(12)	P(3)–B(2)–B(7)	124.5(12)

N.m.r. spectroscopy at low temperatures (see section 3) indicates that this is asymmetric [(**A**), Figure 4] with the hydrogen atom again in an approximately *cisoid* configuration with respect to the three phosphine ligands, but now in one of the conventional 'octahedral' co-ordination sites and with a phosphine ligand occupying the capped position; an asymmetric disposition is also favoured by the iridium analogue, $[6,6,6\text{-}(PPh_3)_2H\text{-}nido\text{-}6\text{-}IrB_9H_{13}]$,[9] and its orthocycloboronated derivatives,[10,11] which however have only three *exo*-polyhedral ligands, $H(PPh_3)_2$, rather than the four, $H(PMe_2Ph)_3$, in the present species. N.m.r. spectroscopy (section 3) also shows that the species is fluxional in solution, with equilibration between the two enantiomeric forms of the structure (**A**) in Figure 4 occurring *via* a non-dissociative pseudorotational process ($\Delta G^{\ddagger}$ *ca.* 35 kJ mol^{-1} at −90 °C) of the three ligands, H, P_a, and P. At higher temperatures the third phosphine ligand, *i.e.* that *trans* to the Re(6)–B(2) bond (P_b), also becomes involved in an extension of this pseudorotational process, with $\Delta G^{\ddagger}$ for this involvement being *ca.* 56 kJ mol^{-1} at 0 °C. Compounds (**2**), (**3**), and (**5**) are all similarly fluxional. The structures of the substituted derivatives of (**1**) readily follow from a comparison of their n.m.r. properties with those of compound (**1**) and also with those of compound (**4**), whose structure is discussed in the following paragraphs.

The crystallographically determined structure of the phosphine-cage-substituted species, $[2\text{-}(PMe_2Ph)\text{-}6,6,6,6\text{-}(PMe_2Ph)_2ClH\text{-}nido\text{-}6\text{-}ReB_9H_{12}]$ (**4**) is shown in Figure 3. This can also be seen to be a *nido*-6-metalladecaborane. Hydrogen atoms were not located in the diffraction analysis but are reasonably assigned to the eight non-phosphinated B-terminal positions. This was confirmed by selective $^1H\text{-}\{^{11}B\}$ n.m.r. spectroscopy which also showed that there are four bridging hydrogen atoms at Re(6)B(7), Re(6)B(5), B(8)B(9), and B(9)B(10) (see section 3 and Table 5). These are again consistent with the *nido* ten-vertex formulation, and the longer distances of B(5)–B(10) and B(7)–B(8) as discussed above confirm this. The geometry about the metal centre, however, differs from that of the other species reported here. N.m.r. spectroscopy indicates

Table 5. Boron-11 and proton n.m.r. data for cluster compounds (**1**)—(**5**) in $CDCl_3$ solution at +20 °C

	(1)		(2)[b]			(3)[c]			(4)			(5)[d]		
Assignment[a]	δ(^{11}B)	δ(^{1}H)	δ(^{11}B)	Δσ[e]	δ(^{1}H)	δ(^{11}B)	Δσ[e]	δ(^{1}H)	δ(^{11}B)	Δσ[e]	δ(^{1}H)	δ(^{11}B)	Δσ[e]	δ(^{1}H)
1, 3	+10.2	+4.51	+3.8	+6.4γ	+4.09	+13.9, +1.8	−3.7γ, +8.4β	+4.70, +4.20	+5.9	+4.3β	+4.45	+11.2	−1.0β	+4.52
5, 7	+12.2	+5.11, −10.74[f]	+14.8	−2.6γ	+5.23, −10.81[f]	+20.4, +1.7	−8.2δ, +10.5β	+5.70, −10.73[f], +4.07, −10.34[f]	+12.7	−0.5β	+5.08, −6.02[g,h]	+10.4	+1.8β	+5.43, −10.65[f]
9	+5.5	+2.60, −4.20	+23.0	−17.5α	—, −2.22	−6.2	−11.7β	+2.33, −1.44[i], −4.02[i]	+0.7	+4.8γ	+2.82, −3.70	+0.2	+5.3γ	+2.43, −4.29
8, 10	−1.5	+2.60, −4.20	−14.9	+13.4β	+2.09, −2.22	+23.0, −16.3	−24.5α, −14.8γ	—, −1.44[i], +1.86, −4.02[i]	−0.7	+0.8γ	+2.57, −3.70	+2.1	−3.6γ	+2.56, −4.29
2	−29.8	−0.30	−33.8	+4.0δ	−0.51	−32.2	+2.4γ	−0.43	−41.8[j,k,l]	+12.0α	—	−15.8	−14.0α	—
4	−29.0	+2.06	−26.2	−3.8β	+2.84	−31.4	+2.4β	+2.17	−32.3	+3.2γ	+2.08	−32.2	+3.2γ	+1.90
(Re)6	—	−5.53[m]	—		−5.47[m]	—		−5.84[m]	—		−10.81[g,j,n]	—		−5.05[m]

[a] See text. [b] CH_3CH_2O at δ 1.58 p.p.m., CH_3CH_2O at δ 3.92 p.p.m., $^3J(^1H^1H)$ unresolved at 21 °C. [c] CH_3CH_2O at δ 1.81 p.p.m., CH_3CH_2O at δ 3.82 p.p.m. (average), $^3J(^1H,^1H)$ *ca.* 7 Hz; the methylene resonance is an ABX_3 pattern arising from the non-equivalence of the two $-CH_2-$ protons on the chiral 8-position. [d] In CD_2Cl_2 solution at +19 °C. [e] Δσ = [δ(^{11}B) of compound (**1**) − δ(^{11}B)] and is the increase in shielding of a boron nucleus in the rhenadecaborane cluster upon substitution of a B-terminal hydrogen in (**1**) by OEt, (**2**) and (**3**); by PMe_2Ph, (**4**); or by Cl (**5**). Greek letters signify position of B atom to the relative substituent. [f] Note no couplings $^2J(^{31}P–Re–^1H_{bridge})$ resolved (in contrast with the ruthenium and iridium analogues; refs. 6 and 9). [g] Small coupling $^2J(^1H_{bridge}–Re–^1H) \leqslant$ *ca.* 2 Hz (from $^1H-\{^1H,^{11}B\}$ experiments). [h] Doublet, splitting 19 Hz, presumably arising from $^2J(^{31}P–Re–^1H)$ (*trans*); in contrast to (**1**), (**2**), (**3**), and (**4**) (footnote *f*). [i] Two bridging B–H–B resonances only, at δ −1.44 and −4.02 p.p.m.; their duplication in the Table signifies that they are correlated with two boron sites B(8)B(9) and B(9)B(10). [j] Sharpening of ReH terminal proton resonance occurs in $^1H-\{^{11}B(2)\}$ experiments indicating small coupling $^2J(^{11}B–Re–^1H)$ of $\leqslant$ *ca.* 2 Hz. [k] $^1J(^{31}P–^{11}B)$ = 140 ± 5 Hz. [l] Selective irradiation of ν[^{11}B(2)] also sharpens P-methyl proton resonances at δ(^{1}H) +0.89 p.p.m. indicating coupling $^3J(^{11}B–P–C–^1H)$ of $\leqslant$ *ca.* 1 Hz. [m] Quartets, arising from couplings $^2J(^{31}P–Re–^1H)$ of *ca.* 50 Hz (Table 6). [n] Doublet [$^3J(^{31}P–B–Re–^1H)$ = 22 Hz] of triplets [$^2J(^{31}P–Re–^1H)$ (*cisoid*) = 44 Hz].

Table 6. Selected phosphorus-31 n.m.r. data for the *nido*-6-rhenadecaboranes (**1**)—(**5**) in $CDCl_3$ solution at −50 °C

	(1)	(2)	(3)	(4)	(5)
$\delta(^{31}P)$/p.p.m.[a,b] {A, B, C}	−16.39 (2)[c,d] −11.56 (1)	−17.48 (2)[c] −11.07 (1)	{−17.61 (1), −14.08 (1)} −11.66 (1)	−34.53 (2) +0.5 (1)[e]	−16.11 (2)[c] −12.25 (1)
θ_c/°C[f]	0 ± 5	15 ± 5	15 ± 5	—	+30 ± 5
$^2J(^{31}P\text{–}Re\text{–}^1H)$(mean)/Hz[g]	*ca.* 50	*ca.* 50	*ca.* 50		*h*
$^2J(^{31}P_A\text{–}Re\text{–}^1H)$/Hz[b]	48 ± 2	50 ± 4	*i*		*i*
$^2J(^{31}P_C\text{–}Re\text{–}^1H)$/Hz[b]	57 ± 2	57 ± 3	*i*		*i*
$^2J(^{31}P_A\text{–}^{31}P_C)$/Hz[b]	*j*	*j*	⩽ *ca.* 2		*ca.* 3
$^2J(^{31}P_B\text{–}^{31}P_C)$/Hz[b]	—	—	*ca.* 8[k]	—	

[a] Relative intensities in parentheses; the phosphorus nuclei exhibited increasing shielding with temperature, $d\sigma/dT$, of *ca.* +0.015 p.p.m. K^{-1} (P_A and P_B) and *ca.* +0.03 p.p.m. K^{-1} (P_C). [b] A, B, C serve to distinguish separate resonances *in this Table only*, and do not necessarily correspond to P_a, P_b *etc.* in Figure 4. [c] A and B equivalent in this compound. [d] At very low temperatures this separates into two resonances [$\delta(^{31}P)$ −10.76 and −19.60 p.p.m. at −95 °C]; coalescence temperature (at 40.25 MHz) −90 °C. [e] Phosphorus atom bonded to cage boron, $^1J(^{31}P\text{–}^{11}B)$ *ca.* 138 Hz. [f] For 40-MHz ^{31}P spectra. [g] At +21 °C; that the magnitude is similar to that of the component *J*'s at low temperature shows that they have the same sign. [h] Peaks unresolved at 100 MHz due to fluxionality. [i] Not measured. [j] Unresolved at −50 °C, $w_{\frac{1}{2}}$ *ca.* 12 Hz. [k] $^2J(^{31}P_A\text{–}^{31}P_B)$ *ca.* 5 Hz.

that the ReH terminal hydrogen atom is again in a symmetrically *cisoid* position relative to the two phosphine ligands, but the significantly different magnitude of the couplings [*ca.* 44 Hz in (**4**) *versus ca.* 50 Hz in (**1**)] now indicates that a somewhat different co-ordination disposition is present. The observed disposition of the other ligands then reasonably indicates that the hydrogen-atom position is as depicted by the hatched lines in Figure 3 and also as depicted in (**C**) of Figure 4, *viz.* in the trigonal gap between P(1), P(2), and B(2) and approximately *trans* to the Re(6)–Cl(1) bond. Consistent with this the angles P(1)–Re(6)–B(2), P(1)–Re(6)–P(2), and P(2)–Re(6)–B(2) are quite large at 120.7, 106.3, and 116.5° respectively and the corresponding angles with Cl(1) [P(1)–Re(6)–Cl(1) and P(2)–Re(6)–Cl(1)] of *ca.* 84° are less than would be expected for an undistorted octahedral environment. These dispositions could also be rationalized on the basis of a seven-orbital capped octahedral bonding geometry [Figure 5(*a*)], but there is considerable distortion from this ideal, and an arrangement such as in Figure 5(*b*) which has a square-pyramidal five-orbital distribution with two additional orbitals emanating from the basal plane and in the molecular C_s mirror plane may be a better description. In either description, the compound is again an 18-electron d^4 rhenium(III) species, now with an effective *arachno*-$[B_9H_{12}(PMe_2Ph)]^-$ ligand co-ordinating in a tridentate manner to the $[Re(H)Cl(PMe_2Ph)_2]^+$ centre. In cluster terms the neutral $Re(H)Cl(PMe_2Ph)_2$ fragment would contribute three orbitals but now only one electron to the cluster bonding scheme. In contrast to compounds (**1**), (**2**), (**3**), and (**5**), which have a different *exo*-polyhedral ligand geometry, we have found no evidence for a fluxional process occurring in this compound in solution.

The seven-orbital bonding configuration as manifested in four *exo*-polyhedral ligands with a more or less classical 'Wadian' three-orbital cluster contribution has only once been previously observed in metallaborane chemistry, *viz.* in the 18-electron d^4 iridium(v) four-vertex *arachno* species $[(PPh_3)_2(CO)HIrB_3H_7]$ (although this may also have some contributions from a six-orbital format).[16] It should be noted that an alternative seven-orbital configuration now with three *exo*-polyhedral ligands and four orbitals involved in cluster bonding is probably involved in a number of other iridaborane and related species. This leads to the interesting series of *isocloso* and *isonido* cluster geometries as discussed elsewhere.[10,17,22]

3. *N.M.R. Behaviour.*—Some aspects of the n.m.r. behaviour have been mentioned in section 2 above; other aspects are discussed here. The n.m.r. behaviour of the blue cage-phosphine-substituted species [2-(PMe_2Ph)-6,6,6,6-$(PMe_2Ph)_2$ClH-*nido*-6-ReB_9H_{12}] (**4**) is straightforward and it is therefore convenient to discuss this first. Phosphorus-31 and proton parameters associated with the rhenium co-ordination environment are given in Tables 5 and 6. These are consistent with the single-crystal molecular structure and with a Re–H hydrogen atom in a position mutually *cis* to the two phosphine ligands and approximately *trans* to the chlorine atom as discussed above [(**C**), Figure 4]. It may be noted that the (*cis*) $^2J(^{31}P\text{–}Re\text{–}^1H)$ coupling of *ca.* 44 Hz differs from the range observed for compounds (**1**), (**2**), (**3**), and (**5**) discussed below which exhibit a different stereochemistry in this region. The incidence of a *cisoid* coupling, $^3J(^1H\text{–}Re\text{–}B\text{–}^{31}P)$, is also of interest, but this now has ample precedent in a variety of metallaborane systems[6,12,15,23] and also in related ones such as the analogous coupling $^3J(^1H\text{–}B\text{–}B\text{–}^1H)$ in *nido*-decaborane itself and its *arachno* derivatives $B_{10}H_{12}L_2$.[24–26] A *cisoid* coupling $^3J(X\text{–}B\text{–}B\text{–}Y)$ is not always observed for this type of configuration, however,[12] and so it obviously has a dependence upon the electronic as well as the geometric structure; any corresponding *gauche* coupling $^3J(^{31}P\text{–}B\text{–}Re\text{–}^{31}P)$ was not resolved in our experiments, indicating an upper limit to this of *ca.* 20 Hz.

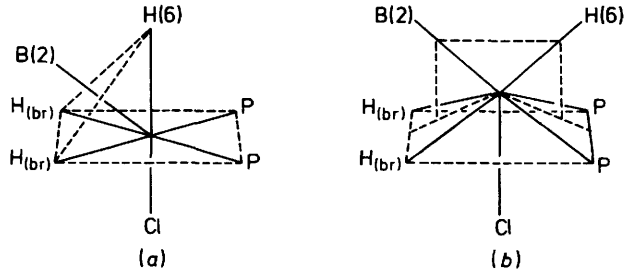

Figure 5. Schematic representation of possible descriptions of the formalized bonding geometry about rhenium in the solid-state structure of $[(PMe_2Ph)_2ClHReB_9H_{12}(2\text{-}PMe_2Ph)]$ (**4**): (*a*) is a capped octahedral configuration of the seven metal bonding orbitals, and (*b*) is a square-pyramidal PPHHCl configuration with the vectors to H(6) and B(2) emanating from the square plane but in the molecular mirror plane (*cf.* Figure 4); the latter configuration thus approximates to a capped trigonal-prismatic disposition of bonding orbitals

The cluster boron-11 and proton resonances of the blue compound (**4**) are given in Table 5 and the boron-11 spectrum is shown in Figure 6. These are again consistent with the crystal molecular structure and are readily assigned *via* peak multiplicity, selective sharpening of bridging proton resonances

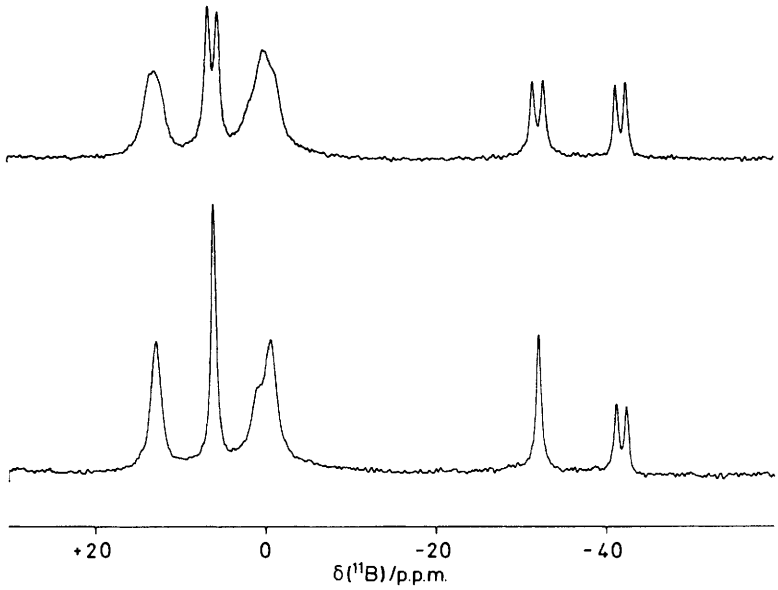

Figure 6. 115.5-MHz ^{11}B (upper trace) and ^{11}B-{^{1}H(broad-band noise)} (lower trace) n.m.r. spectra for $[(PMe_2Ph)_2HClReB_9H_{12}(2\text{-}PMe_2Ph)]$ (**4**). The doublet structure arising from the coupling $^{1}J(^{31}P\text{–}^{11}B)$ of *ca.* 140 Hz is readily apparent on the B(2) resonance in the lower trace at −41.8 p.p.m.

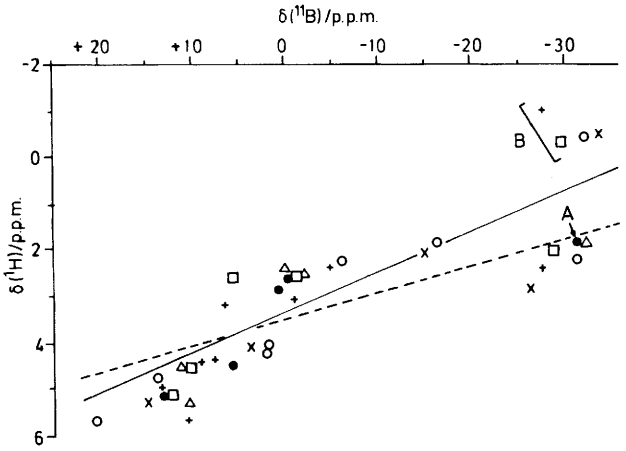

Figure 7. Proton–boron-11 shielding correlation plot for the *exo*-terminal hydrogen atoms of compounds (**1**) (□), (**2**) (×), (**3**) (○), (**4**) (●), (**5**) (△), and for comparison purposes, the 6-iridadecaborane analogue $[(PPh_3)_2HIrB_9H_{13}]$ (+) (ref. 9). The (2,4) correlation point A [compound (**4**)] has no equivalent at B, which therefore assigns the latter resonances to the 2-positions, and the resonances grouped around A to the 4-positions. The slopes drawn represent the ratios $\delta(^{11}B):\delta(^{1}H)$ 16:1 (– – –) and 12.5:1 (———) (see text)

in ^{1}H-{^{11}B} experiments, and by comparison with known[4–9] *nido*-6-metalladecaboranyl systems. As with compounds (**1**), (**2**), (**3**), and (**5**) (see below) there is a general parallel between the boron-11 and proton shieldings of directly bound terminal hydrogen atoms (Figure 7). The gradient of this correlation of $\delta(^{11}B):\delta(^{1}H)$ is *ca.* 12.5:1. Although this is similar to that observed for the iridium analogue $[6,6,6\text{-}(PPh_3)_2H\text{-}nido\text{-}6\text{-}IrB_9H_{13}]$[9] (also included in Figure 6 for comparison) it is of interest that it is somewhat less than the slope of *ca.* 16:1 observed for other decaboranyl derivatives and a variety of other species.[25–32] This is discussed in further detail below.

The n.m.r. behaviour of compounds (**1**), (**2**), (**3**), and (**5**), which have a $ReH(PMe_2Ph)_3$ metal centre rather than a $Re(H)Cl(PMe_2Ph)_2$ metal centre, is less straightforward in that the temperature variation of the non-borane parameters indicates that the $ReH(PMe_2Ph)_3$ co-ordination environment is fluxional in solution. Retention of coupling shows that this is a non-dissociative scrambling of the non-borane ligands on the metal centre. This may be grouped into two sub-processes as indicated by the n.m.r. behaviour of the non-borane ligands on the rhenium atom (Tables 5 and 6). At high temperatures (> +25 °C) all the phosphine ligands are, on time-average, equivalent. In view of the low-temperature static form (see below) this probably occurs *via* a classical Berry-type pseudo-rotational process in which all four ligands may occupy all four co-ordination positions, probably with a tendency for the hydrogen atom not to favour the *endo*-terminal and capping sites. At intermediate temperatures (*ca.* −50 °C) one of the phosphine ligands becomes fixed, probably in the *endo*-terminal position [P(2) in the solid-state structure]; the activation energy for the incorporation of this phosphine into the fluxional process can be estimated from the n.m.r. peak coalescence temperatures, particularly in the phosphorus-31 spectra, and is in the range 45—60 kJ mol^{-1} for the four compounds (**1**), (**2**), (**3**), and (**5**) studied.* The other two phosphine ligands and the hydride ligand meanwhile remain fluxional *via* mutual exchange, presumably again *via* a straightforward pseudorotational process. This will be among the three remaining sites, and presumably occurs principally between the two asymmetric forms (A) and (C) shown in Figure 8 (see following paragraph). That the mean magnitude of the couplings $^{2}J(^{31}P\text{–}Re\text{–}^{1}H)$ for all three phosphines is similar both above and below the coalescence temperatures indicates they are all of the same sign and therefore in a similar geometric disposition with respect to the hydrogen atoms.

At lower temperatures (−95 °C) this fluxionality is in turn

* The rate analysis of the exchange processes is confused by two effects: (*a*) the presence of quadrupolar coupling effects of the boron nuclei on the phosphorus resonances, which are different for the two different phosphorus environments in each case, and which result in broadening due to unresolved coupling at higher temperatures; (*b*) the presence of significant temperature effects on the shielding of the phosphorus nuclei, $d\sigma/dT$, of up to +0.03 p.p.m. K^{-1}, which again are different for the different phosphorus environments in each case, and may be due to changes with temperature in the mean bond rotamer populations.

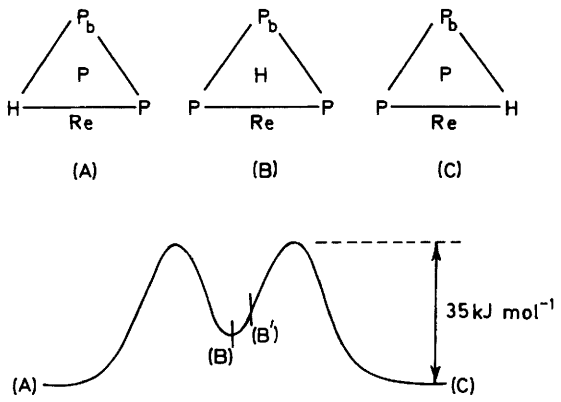

Figure 8. Representation of the non-borane ligand dispositions associated with the lower-temperature fluxional processes in compounds (**1**), (**2**), (**3**), and (**5**) in which the phosphorus atom P_b remains static. (A) and (C) represent enantiomeric forms most stable in solution, and (B) is as found in the solid-state structure of compound (**1**) (see also Figure 4). (B) must represent a reasonably stable intermediate in the (A) $\rightleftharpoons$ (C) pseudorotational fluxional process as represented on the reaction co-ordinate. In fact the solid-state structure of compound (**1**) does not quite represent the C_s minimum as there is a slight twist (Table 1 and Figure 2); it is therefore some way along the reaction co-ordinate (B')

slowed ($\Delta G^{\ddagger}$ *ca.* 30 kJ mol^{-1}), with the $\delta(^{31}P)$ data (Table 6) showing that the asymmetric form, (A) and (C) in Figure 8, is the most stable species in solution. It is of interest that the molecular structure observed in the crystal [Figure 2, and (B) in Figure 8] is not that observed in solution, although this will undoubtedly represent a reasonably stable intermediate in the fluxional process (schematic reaction co-ordinate in Figure 8).

As far as n.m.r. measurements are concerned, the exchange process in solution at intermediate and higher temperatures between the two enantiomeric forms gives the compounds (**1**), (**2**), (**3**), and (**5**) a time-averaged structure of effective C_s mirror-plane symmetry. This is how the cluster boron-11 and proton n.m.r. data for these compounds are presented in Table 5. For example, the boron-11 resonance intensity pattern for compound (**1**) is 1:2:2:2:1:1 rather than having the nine separate resonance positions required from the non-exchanging racemic mixture. Similar considerations for the diastereoisomeric species, [6,6,6,6-$(PMe_2Ph)_3$H-8-(OEt)-*nido*-6-ReB_9H_{12}] (**3**) determine that only nine resonance positions are observed in the boron-11 spectrum at higher temperatures, rather than the 18 expected for the mixture of non-exchanging diastereoisomeric forms. Comparison with the static asymmetric iridium species [6,6,6-$(PPh_3)_2$H-*nido*-6-IrB_9H_{13}][9] indicates that the metal–hydride *versus* metal–phosphine *trans* effect in the low-temperature static forms would induce differences of up to *ca.* 5 p.p.m. on the boron nuclear shielding. We have not yet been able to investigate this phenomenon in the rhenium compounds, however, because the boron-11 resonances are so broadened at lower temperatures by efficient quadrupolar relaxation that we have not been able to distinguish the individual resonances resulting from the 'freezing-out' of the low-temperature process; only in the phosphorus-31 spectrum is this readily distinguishable on the equipment available.

As mentioned above for compound (**4**), there is also an approximate correlation for compounds (**1**), (**2**), (**3**), and (**5**) between the proton shielding of the *exo*-terminal protons and the nuclear shielding of the cluster boron atoms to which they are directly bound; this has a slope of $\delta(^{11}B):\delta(^{1}H)$ of *ca.* 12.5:1 (solid line in Figure 7). This slope differs from that of 16:1 observed for a variety of other borane and metallaborane species.[24–32] If the B(2)H(2) data are excluded, however, then the correlation with a slope of 16:1 becomes more reasonable (hatched line in Figure 7); this would suggest an anomalous shielding behaviour for the 2-position next to the metal centre, which is perhaps not unexpected.

Experimental

General.—The starting rhenium(III) complex, yellow *mer*-$[ReCl_3(PMe_2Ph)_3]$, was prepared from $NaReO_4$ by standard methods.[33] $B_{10}H_{14}$ was sublimed (0.1 mmHg/80 °C) before use and $[NEt_4][B_9H_{14}]$ was prepared from it by published methods.[34] Absolute ethanol was used as supplied and CH_2Cl_2 was refluxed over and distilled from CaH_2 before use. Nitrogen gas was dried by passage through concentrated H_2SO_4 and then through KOH pellets.

Nuclear Magnetic Resonance Spectroscopy.—100-MHz ^1H, ^1H-$\{^{11}B\}$, and ^1H-$\{^{31}P\}$, 32-MHz ^{11}B and ^{11}B-$\{^1H\}$, and 40-MHz ^{31}P-$\{^1H\}$ n.m.r. experiments were carried out on a JEOL FX-100 pulse Fourier-transform (F.t.) spectrometer. 128-MHz ^{11}B and ^{11}B-$\{^1H\}$ experiments were performed on a Bruker WH-400 pulse (F.t.) spectrometer at the S.E.R.C. service centre at Sheffield University. 115.5-MHz ^{11}B and 360-MHz ^1H-$\{^{11}B\}$ n.m.r. experiments were performed at the Edinburgh University S.E.R.C. service centre on a Bruker WH-360 pulse (F.t.) spectrometer. Solutions and conditions are specified in Tables 1 and 2. Chemical shifts (δ) are given in p.p.m. to high frequency (low field) of $SiMe_4$ for ^1H, to high frequency of $BF_3{\cdot}OEt_2$ in $CDCl_3$ [Ξ 32 083 971 Hz] for ^{11}B,[25] and to high frequency of 85% H_3PO_4 [Ξ 40 480 730 Hz] for ^{31}P.

Reaction of mer-$[ReCl_3(PMe_2Ph)_3]$ *with* $[NEt_4][B_9H_{14}]$.—In deoxygenated absolute ethanol (25 cm^3) under dry nitrogen was suspended $[NEt_4][B_9H_{14}]$ (2 mmol, 428 mg). Solid *mer*-$[ReCl_3(PMe_2Ph)_3]$ (0.2 mmol, 140 mg) was added to this by use of a 'tipper' tube, and the reaction mixture was heated under reflux for 1.5 h under an atmosphere of dry nitrogen gas. Subsequent manipulations were carried out in air. The reaction mixture was evaporated to dryness (30 °C, water pump) and redissolved in *ca.* 10 cm^3 of dry CH_2Cl_2. This solution was then applied to a series of preparative t.l.c. plates (20 × 20 × 0.1 cm; silica, Keiselgel GF 254, made in these laboratories as required) and eluted with CH_2Cl_2 (100%). Four main coloured bands were readily distinguished, with R_f values of 0.9 (purple), 0.7 (orange), 0.5 (purple), and 0.3 (yellow). These were removed from the plates, and separated from the silica by washing with *ca.* 25 cm^3 of dry CH_2Cl_2 per component. Further repeated chromatography of each component using the same solvent system yielded each component in a pure state, and an additional compound [R_f 0.85 (blue), compound (**4**)] was also obtained in small amounts (*ca.* 1 mg; <1%). The yellow compound (R_f 0.3) was identified as unreacted starting rhenium complex (43 mg; 30% recovery). The major purple component (at R_f 0.9) was recrystallized from CH_2Cl_2–cyclohexane and an air-stable purple microcrystalline solid [identified as compound (**1**), see text] was obtained in 40% yield (40 mg). Single crystals of both compounds (**1**) and (**4**) suitable for *X*-ray diffraction analysis were grown by diffusion of solvents (CH_2Cl_2–cyclohexane). The orange band (R_f 0.7) was obtained as an air-stable orange-brown microcrystalline solid [compound (**2**)] and the lower purple band (R_f 0.5) was obtained as a purple microcrystalline solid [compound (**3**)] in yields of 25% (25 mg) and 4% (3 mg) respectively. The yields quoted are based on a 70% conversion of the starting rhenium complex [Found for (**1**): C, 40.25; H, 6.50; B, 13.25; P, 13.1; Re (by difference), 26.9. $C_{24}H_{47}B_9P_3Re$ requires C, 40.55; H, 6.75; B, 13.70; P, 12.95; Re, 26.1%. Found for (**2**): C, 41.20; H, 6.75; B, 13.05; P, 12.45; Re + O (by difference), 26.55. $C_{26}H_{51}B_9OP_3Re$ requires C,

Table 7. Atom co-ordinates ($\times 10^4$) for compound (**1**)

Atom	*x*	*y*	*z*
B(1)	2 320(2)	4 683(4)	7 570(4)
B(2)	2 657(2)	2 963(4)	6 858(4)
B(3)	1 997(2)	3 338(4)	8 366(4)
B(4)	1 447(2)	4 535(4)	8 322(5)
B(5)	2 525(2)	3 701(4)	5 489(4)
Re(6)	2 434	1 046	4 171
B(7)	1 962(2)	1 493(4)	6 794(4)
B(8)	1 152(2)	2 572(4)	7 716(5)
B(9)	897(2)	3 569(4)	6 726(5)
B(10)	1 661(2)	4 738(4)	6 509(5)
P(1)	3 344	1 492(1)	2 438(1)
P(2)	1 534	−65(1)	2 315(1)
P(3)	2 943	−688(1)	4 659(1)
C(11)	3 256(2)	2 823(5)	1 630(5)
C(12)	3 507(2)	−134(4)	513(4)
C(131)	4 230(1)	2 245(2)	3 266(2)
C(132)	4 808(1)	2 055(2)	2 245(2)
C(133)	5 463(1)	2 617(2)	2 896(2)
C(134)	5 539(1)	3 368(2)	4 568(2)
C(135)	4 961(1)	3 557(2)	5 589(2)
C(136)	4 306(1)	2 996(2)	4 938(2)
C(21)	986(2)	−1 675(4)	2 472(6)
C(22)	1 692(2)	−864(5)	124(4)
C(231)	921(1)	1 186(3)	2 528(3)
C(232)	1 146(1)	2 370(3)	2 111(3)
C(233)	690(1)	3 296(3)	2 185(3)
C(234)	9(1)	3 039(3)	2 676(3)
C(235)	−216(1)	1 855(3)	3 093(3)
C(236)	240(1)	929(3)	3 019(3)
C(31)	3 466(3)	126(6)	6 482(5)
C(32)	2 350(3)	−2 193(6)	4 931(8)
C(331)	3 545(1)	−1 761(2)	3 085(2)
C(332)	4 243(1)	−1 179(2)	3 162(2)
C(333)	4 692(1)	−1 970(2)	1 952(3)
C(334)	4 443(1)	−3 344(2)	676(2)
C(335)	3 744(1)	−3 926(2)	609(2)
C(336)	3 295(1)	−3 135(2)	1 819(2)

Table 8. Hydrogen atom co-ordinates ($\times 10^4$) for compound (**1**)

Atom	*x*	*y*	*z*
H(1)	2 706(15)	5 719(35)	8 265(37)
H(2)	3 168(21)	3 243(42)	7 386(47)
H(3)	2 059(17)	3 481(37)	9 572(41)
H(4)	1 250(20)	5 281(43)	9 470(47)
H(5)	2 944(17)	4 496(36)	5 091(38)
H(7)	1 977(17)	726(36)	7 325(39)
H(8)	805(22)	2 161(44)	8 384(48)
H(9)	331(21)	3 580(43)	6 725(48)
H(10)	1 641(20)	5 734(43)	6 281(46)
H(5,6)	2 183(16)	2 696(33)	4 252(37)
H(6,7)	1 775(21)	866(45)	5 354(49)
H(8,9)	1 006(19)	2 199(42)	6 296(44)
H(9,10)	1 265(21)	3 552(46)	5 559(49)
H(11a)	3 677(22)	2 983(43)	981(49)
H(11b)	3 125(24)	3 598(53)	2 406(56)
H(11c)	2 842(24)	2 342(47)	734(53)
H(12a)	3 680(23)	−817(50)	734(53)
H(12b)	3 737(22)	118(44)	−248(51)
H(12c)	3 107(23)	−519(47)	−44(52)
H(132)	4 740(19)	1 458(42)	970(46)
H(133)	5 891(23)	2 568(48)	2 268(51)
H(134)	5 977(21)	3 685(45)	5 068(50)
H(135)	4 995(19)	4 157(41)	6 835(44)
H(136)	3 944(25)	3 066(55)	5 604(58)
H(21a)	858(19)	−1 361(41)	3 518(49)
H(21b)	587(20)	−2 066(41)	1 783(45)
H(21c)	1 312(20)	−2 472(42)	2 115(44)
H(22a)	1 924(18)	25(41)	−97(40)
H(22b)	1 878(23)	−1 707(51)	−308(53)
H(22c)	1 244(25)	−1 292(49)	−334(53)
H(232)	1 643(23)	2 506(48)	1 581(51)
H(233)	917(28)	4 171(61)	1 849(67)
H(234)	−225(29)	3 602(63)	2 564(67)
H(235)	−694(29)	1 641(61)	3 338(67)
H(236)	64(21)	151(44)	3 313(47)
H(31a)	3 178(25)	557(54)	7 519(61)
H(31b)	3 594(29)	−763(66)	6 631(66)
H(31c)	3 867(35)	858(76)	6 424(79)
H(32a)	2 083(21)	−2 863(48)	3 964(53)
H(32b)	2 618(23)	−2 859(51)	5 055(52)
H(32c)	2 107(40)	−1 971(77)	5 788(88)
H(332)	4 398(18)	−230(39)	4 034(42)
H(333)	5 203(22)	−1 511(43)	1 995(47)
H(334)	4 721(23)	−3 841(48)	−194(52)
H(335)	3 600(24)	−4 754(53)	−311(56)
H(336)	2 795(22)	−3 460(46)	1 776(51)

41.35; H, 6.75; B, 12.85; P, 12.30; Re + O, 26.7%]. N and Cl were shown to be absent from both compounds.

Reaction of $[(PMe_2Ph)_3HReB_9H_{13}]$ (**1**) *in Refluxing Ethanol.*—To deoxygenated absolute ethanol (25 cm^3) under dry nitrogen gas was added compound (**1**) (26 mg). The solution was heated to reflux for 1.5 h. Separation of the reaction mixture as above yielded compounds (**1**) (7 mg), (**2**) (1 mg), and (**3**) (1 mg). The yields of compounds (**2**) and (**3**) based on a 75% conversion are therefore *ca.* 5% each.

Thermolysis of $[(PMe_2Ph)_3HReB_9H_{13}]$ (**1**) *in* $C_2D_2Cl_4$ *Solution.*—A small sample of compound (**1**) (*ca.* 10 mg) in a 5-mm n.m.r. tube, with *sym*-$C_2D_2Cl_4$ as solvent, was kept at 100 °C for 15 min in the spectrometer whilst its ^{31}P-$\{^1H\}$ n.m.r. spectrum was monitored. The resonance associated with compound (**1**) (δ −15.58 p.p.m.) disappeared during this time and was replaced by a new resonance (δ −19.09) which was observed to build up as compound (**1**) decreased. Evaporation of the solvent (90 °C, water pump) followed by preparative t.l.c. (100% CH_2Cl_2 as eluant) then yielded a purple compound (R_f 0.85) in quantitative yield [compound (**5**)]. The n.m.r. properties of compound (**5**) are summarized in Tables 5 and 6; its characterisation is described in the Results and Discussion section.

Crystallographic Studies.—All intensity data were recorded on a Syntex $P2_1$ diffractometer operating in the ω–2θ scan mode with graphite monochromatised Mo-K_α radiation (λ = 71.069 pm), according to a procedure described in detail elsewhere.[35] The data for both compounds were corrected for absorption empirically.[36] The structure for compound (**1**) was determined routinely by Patterson and Fourier difference syntheses. For compound (**4**), however, although the heavy-atom position could be readily located from a Patterson synthesis, problems with pseudo-symmetry were encountered when using the more standard Fourier difference methods. Hence the rest of the structure was determined by the application of direct methods on difference structure factors.[37] Both structures were refined by full-matrix least squares using the SHELX program system.[38] For compound (**4**) only the Re, Cl, and P atoms were assigned anisotropic thermal parameters and consequently no hydrogen atoms were located in a subsequent difference synthesis. For compound (**1**) all non-hydrogen atoms were assigned anisotropic thermal parameters and all hydrogen atoms except the hydride attached to the Re atom were located experimentally. These were refined freely with individual isotropic parameters. For compound (**4**) unit weights were used whilst for compound (**1**) the weighting scheme $w = 1/[\sigma^2(F_o) +$

Table 9. Atom co-ordinates ($\times 10^4$) for compound (**4**)

Atom	*x*	*y*	*z*
B(1)	10 662(16)	3 285(12)	439(10)
B(2)	10 721(15)	3 217(11)	1 425(9)
B(3)	11 894(16)	3 713(11)	1 103(10)
B(4)	12 116(19)	3 319(13)	227(12)
B(5)	10 130(16)	2 398(12)	801(11)
Re(6)	11 000	1 969	2 000
B(7)	12 206(16)	3 099(11)	1 910(10)
B(8)	13 136(19)	3 140(13)	1 076(12)
B(9)	12 734(20)	2 367(14)	365(13)
B(10)	11 180(18)	2 437(13)	23(12)
P(1)	9 427(4)	1 081(3)	1 939(3)
P(2)	12 104(4)	1 949(3)	3 290(3)
P(3)	9 654(4)	4 005(3)	1 682(2)
Cl(1)	12 112(4)	711(3)	1 893(3)
C(111)	8 061(9)	1 525(7)	2 054(7)
C(112)	7 131(9)	1 644(7)	1 445(7)
C(113)	6 118(9)	2 017(7)	1 544(7)
C(114)	6 035(9)	2 271(7)	2 253(7)
C(115)	6 965(9)	2 152(7)	2 862(7)
C(116)	7 978(9)	1 779(7)	2 763(7)
C(12)	9 591(18)	215(13)	2 582(12)
C(13)	9 050(19)	530(13)	1 030(12)
C(211)	11 719(13)	1 187(8)	3 930(8)
C(212)	12 190(13)	416(8)	3 947(8)
C(213)	11 842(13)	−180(8)	4 384(8)
C(214)	11 024(13)	−6(8)	4 802(8)
C(215)	10 554(13)	765(8)	4 785(8)
C(216)	10 901(13)	1 361(8)	4 348(8)
C(22)	13 649(17)	1 797(12)	3 412(11)
C(23)	12 111(20)	2 877(14)	3 834(13)
C(311)	10 060(11)	4 301(8)	2 667(5)
C(312)	9 448(11)	4 033(8)	3 187(5)
C(313)	9 803(11)	4 262(8)	3 933(5)
C(314)	10 770(11)	4 760(8)	4 159(5)
C(315)	11 382(11)	5 028(8)	3 639(5)
C(316)	11 027(11)	4 798(8)	2 894(5)
C(32)	9 614(17)	4 951(12)	1 164(11)
C(33)	8 172(16)	3 601(12)	1 488(11)

$g(F_o)^2$] was used in which the parameter g was included in refinement to give acceptable agreement analyses.

Crystal data for $[(PMe_2Ph)_3HReB_9H_{13}]$ (**1**). $C_{24}H_{47}B_9P_3Re$, M = 711.6, triclinic, a = 1 984.7(5), b = 1 007.5(2), c = 926.7(2) pm, α = 116.75(1), β = 84.05(2), γ = 101.01(2)°, U = 1.6239 nm^3, space group $P\bar{1}$, Z = 2, D_c = 1.45 g cm^{-3}, μ(Mo-K_α) = 37.21, $F(000)$ = 711.95, T = 290 K. Data collection: scans from 1° below K_{α_1} to 1° above K_{α_2}, scan speeds 1—29.3° min^{-1}, $4.0 < 2\theta < 50.0°$, 5 599 unique data, 5 433 observed [$I > 2\sigma(I)$]. Structure refinement: number of parameters = 482, weighting factor g = 0.0001, R = 0.0202, R' = 0.0205.

Crystal data for $[(PMe_2Ph)_2ClHReB_9H_{12}(PMe_2Ph)]$ (**4**). $C_{24}H_{46}B_9ClP_3Re$, M = 746.6, monoclinic, a = 1 180.3(3), b = 1 663.6(4), c = 1 840.3(4) pm, β = 103.04(2)°, U = 3.5203 nm^3, space group Cc, Z = 4, D_c = 1.41 g cm^{-3}, μ(Mo-K_α) = 35.5 cm^{-1}, $F(000)$ = 1 487.9, T = 290 K. Data collection: scans from 1° below K_{α_1} to 1° above K_{α_2}, scan speeds 2.0—29.3° min^{-1}, $4.0 < 2\theta < 45.0°$, 2 402 unique data, 2 254 observed [$I > 2\sigma(I)$]. Structure refinement: number of parameters = 140, unit weights, R = 0.0365.

Lists of final atomic co-ordinates for compound (**1**) are given in Tables 7 and 8 and for compound (**4**) in Table 9. Selected molecular dimensions are in Tables 1—4.

Acknowledgements

We thank the S.E.R.C. for support, Dr. D. Reed (Edinburgh) for services in high-field n.m.r. spectroscopy, and Mr. A. Hedley for microanalysis.

References

1 R. N. Grimes, in 'Comprehensive Organometallic Chemistry,' eds. G. Wilkinson, F. G. A. Stone, and E. W. Abel, Pergamon Press, Oxford, 1982, vol. 1, pp. 459—542.
2 K. B. Gilbert, S. K. Boocock, and S. G. Shore, in 'Comprehensive Organometallic Chemistry,' eds. G. Wilkinson, F. G. A. Stone, and E. W. Abel, Pergamon Press, Oxford, 1982, vol. 6, pp. 879—946.
3 J. D. Kennedy and N. N. Greenwood, in 'Metal Interactions with Boron Clusters,' ed. R. N. Grimes, Plenum, London, 1982, ch. 2, pp. 43—118.
4 J. W. Lott, D. F. Gaines, H. Schenhav, and R. Schaeffer, *J. Am. Chem. Soc.*, 1973, **95**, 3042.
5 J. W. Lott and D. F. Gaines, *Inorg. Chem.*, 1974, **13**, 2261.
6 J. D. Kennedy, N. N. Greenwood, J. D. Woollins, and M. Thornton-Pett, *J. Chem. Soc., Dalton Trans.*, in the press.
7 G. J. Zimmerman, L. W. Hall, and L. G. Sneddon, *Inorg. Chem.*, 1980, **19**, 3642.
8 T. L. Venable and R. N. Grimes, *Inorg. Chem.*, 1982, **21**, 887.
9 S. K. Boocock, J. Bould, N. N. Greenwood, J. D. Kennedy, and W. S. McDonald, *J. Chem. Soc., Dalton Trans.*, 1982, 713.
10 J. Bould, N. N. Greenwood, J. D. Kennedy, and W. S. McDonald, *J. Chem. Soc., Chem. Commun.*, 1982, 465.
11 J. Bould, Ph.D. Thesis, University of Leeds, 1983; and unpublished work, 1980—1983.
12 J. Bould, N. N. Greenwood, and J. D. Kennedy, *J. Chem. Soc., Dalton Trans.*, 1984, 2477.
13 J. Bould, J. E. Crook, N. N. Greenwood, J. D. Kennedy, and W. S. McDonald, *J. Chem. Soc., Chem. Commun.*, 1982, 346.
14 J. E. Crook, N. N. Greenwood, J. D. Kennedy, and W. S. McDonald, *J. Chem. Soc., Chem. Commun.*, 1983, 83.
15 N. W. Alcock, J. G. Taylor, and M. G. H. Wallbridge, *J. Chem. Soc., Chem. Commun.*, 1983, 1168.
16 J. Bould, N. N. Greenwood, J. D. Kennedy, and W. S. McDonald, *J. Chem. Soc., Dalton Trans*, in the press.
17 J. E. Crook, M. Elrington, N. N. Greenwood, J. D. Kennedy, and J. D. Woollins, *Polyhedron*, 1984, **3**, 901.
18 A. Tippe and W. C. Hamilton, *Inorg. Chem.*, 1969, **8**, 464.
19 M. A. Beckett, J. E. Crook, N. N. Greenwood, J. D. Kennedy, and W. S. McDonald, *J. Chem. Soc., Chem. Commun.*, 1982, 552.
20 J. Bould, J. E. Crook, N. N. Greenwood, and J. D. Kennedy, *J. Chem. Soc., Chem. Commun.*, 1983, 951.
21 L. Aslanov, R. Mason, A. G. Wheeler, and P. O. Whimp, *Chem. Commun.*, 1970, 30.
22 J. E. Crook, N. N. Greenwood, J. D. Kennedy, and W. S. McDonald, *J. Chem. Soc., Chem. Commun.*, 1981, 933.
23 J. E. Crook, N. N. Greenwood, J. D. Kennedy, and W. S. McDonald, *J. Chem. Soc., Chem. Commun.*, 1982, 383.
24 J. E. Crook, N. N. Greenwood, J. D. Kennedy, and W. S. McDonald, *J. Chem. Soc., Dalton Trans.*, 1984, 2487.
25 J. D. Kennedy, in 'N.M.R. in Inorganic and Organometallic Chemistry,' ed. J. Mason, Plenum, London, 1985, ch. 8.
26 J. Rogozinski, unpublished work, University of Leeds, 1983—1984.
27 R. F. Sprecher, B. E. Aufderheide, G. W. Luther III, and J. C. Carter, *J. Am. Chem. Soc.*, 1974, **96**, 4404.
28 R. F. Sprecher and B. E. Aufderheide, *Inorg. Chem.*, 1974, **13**, 2287.
29 R. Ahmed, Ph.D. Thesis, University of Leeds, 1982.
30 N. N. Greenwood, M. J. Hails, J. D. Kennedy, and W. S. McDonald, *J. Chem. Soc., Dalton Trans.*, 1985, 953.
31 J. D. Kennedy and N. N. Greenwood, *Inorg. Chim. Acta*, 1980, **38**, 93.
32 M. A. Beckett, N. N. Greenwood, J. D. Kennedy, and M. Thornton-Pett, *Polyhedron*, in the press.
33 P. G. Douglas and B. L. Shaw, *J. Chem. Soc. A*, 1969, 1491.
34 S. K. Boocock, N. N. Greenwood, M. J. Hails, J. D. Kennedy, and W. S. McDonald, *J. Chem. Soc., Dalton Trans.*, 1981, 1415.
35 A. Modinos and P. Woodward, *J. Chem. Soc., Dalton Trans.*, 1974, 2065.
36 N. Walker and D. Stuart, *Acta Crystallogr., Sect. A*, 1983, **39**, 158.
37 For more details, see P. A. J. Prick, P. T. Beurskens, and R. O. Gould, *Acta Crystallogr., Sect. A*, 1983, **39**, 570.
38 G. M. Sheldrick, SHELX 76, Program System for *X*-Ray Structure Determination, University of Cambridge, 1976.

Received 2nd July 1984; *Paper* 4/1127